1996ApJ...469..554C

THE ASTROPHYSICAL JOURNAL, 469:554–563, 1996 October 1
© 1996. The American Astronomical Society. All rights reserved. Printed in U.S.A.

RADIO OUTFLOWS AND THE ORIGIN OF THE NARROW-LINE REGION IN SEYFERT GALAXIES[1]

A. CAPETTI,[2] D. J. AXON,[2,3] F. MACCHETTO,[2,3] W. B. SPARKS,[2] AND A. BOKSENBERG[4]

Received 1995 August 29; accepted 1995 December 4

ABSTRACT

We present the results of *Hubble Space Telescope* medium-band imaging of four Seyfert 2 galaxies, Mrk 573, Mrk 348, Mrk 3, and Mrk 78, which show extended radio emission, and ground based Johnson *R* images of Mrk 3 and Mrk 78 obtained with the William Herschel Telescope. Together these two data sets allow us to investigate the relationship between the narrow-line region (NLR) emission structure, the radio structure, and the large-scale morphology of the host galaxy.

In all four objects there is a close association between the NLR emission-line morphology and that of the radio emission. Furthermore, it appears that the NLR takes a different form depending on the structure of the radio emission. The emission-line regions associated with the radio lobes are shell-like or bow shock–like, while those associated with the jets are linear.

In Mrk 573, the emission-line ratios [O III]/[O II] and [O III]/Hα show only a slow increase with radius between the bow shocks ([O III]/[O II] ~ 3 and [O III]/Hα ~ 1.5, $r < 2''$) and the outer filaments [O III]/[O II] ~ 4 and [O III]/Hα ~ 2, $2'' < r < 4''$). A similar, but more substantial, trend for increasing ionization with radius is seen in Mrk 78 ([O III]/[O II] ~ 1.4 in the core and [O III]/[O II] ~ 2.9 in the western lobe). In the case of Mrk 573, it appears that a local source of ionization is required to explain the observed ionization structure.

We interpret these results as strong evidence that the line-emitting gas is compressed by the shocks created by the passage of the radio-emitting outflow. The increase in the density due to the shocks causes the line emission to be highly enhanced in the region in which this interaction occurs. The shell-like morphology of the emission-line gas associated with the radio lobes is formed by the sweeping-up of material by the ejected and expanding lobes, while the linear structure associated with the jets arises due to the lateral expansion of hot gas around the jet axis.

There is no evidence for an unresolved bright core which could be identified as the active nucleus in any of these galaxies. From this, we conclude that the nucleus must be hidden along our line of sight. In all four objects, an absorption lane crossing the nuclear region has been detected. In Mrk 348, Mrk 573, and Mrk 3, the typical scale height of the dust lane is less than 50 pc, while in Mrk 78 it is ~ 180 pc. We suggest that these dust lanes are associated with the obscuring torus which occults the Seyfert nucleus.

Three of the objects (Mrk 573, Mrk 3, and Mrk 78) show large-scale stellar bars, and Mrk 573 also shows an inner bar oriented nearly perpendicular to the outer bar. We discuss the relationship between the bars and the orientation of the NLR.

Subject headings: galaxies: active — galaxies: Seyfert — galaxies: structure — infrared: galaxies — radio continuum: galaxies

1. INTRODUCTION

For many years it has generally been accepted that in the narrow-line region (NLR) of Seyfert galaxies the gas is photoionized by nuclear radiation (e.g., Ferland & Osterbrock 1986). The discovery of an NLR with "conelike" morphologies in initial *HST* observations of three nearby Seyfert galaxies (NGC 1068, Evans et al. 1991; NGC 4151, Evans et al. 1993; NGC 5728, Wilson et al. 1993) seemed to give further weight to this long-standing view.

However, ground-based studies have shown that the NLR is inevitably cospatial with the radio emission (Wilson & Ulvestad 1983; Haniff, Wilson, & Ward 1988), and its kinematics clearly display signs of the effect of interactions with the ejected radio-plasma (Whittle et al. 1988; Baldwin, Wilson, & Whittle 1987; Pedlar et al. 1989). This association between the radio-emitting components and the NLR prompted Pedlar et al. (1989) and Taylor, Dyson, & Axon (1992) to argue that the structure of the NLR is dominated by the compression and heating of the interstellar gas generated by shock waves formed by the supersonic radio ejecta. The shock waves can be responsible for the ionization of the thermal gas (Axon, Dyson, & Pedlar 1993, and references therein) and can also create significant continuum emission. As Sutherland, Bicknell, & Dopita (1993) have argued, this locally produced continuum can also be important in ionizing the NLR.

Recently, this physical picture of the NLR received strong support from the pre-COSTAR *HST* observations of the Seyfert 2 galaxy Mrk 3 (Capetti et al. 1995a), which shows a linear NLR cospatial with the radio jets, rather than a conelike morphology. Furthermore, Capetti et al. found kinematic evidence for an interaction between the emitting gas and the radio-jets. One of the most important results they presented in favor of the interaction scenario for the origin of the NLR was that the ionization parameter sensitive line ratios [O III]/[O II] and [O III]/Hα were effectively constant

[1] Based on observations with the NASA/ESA Hubble Space Telescope, obtained at the Space Telescope Science Institute, which is operated by AURA, Inc, under NASA contract NAS 5-26555.

[2] Space Telescope Science Institute, 3700 San Martin Drive, Baltimore, MD 21218.

[3] Astrophysics Division, Space Science Department of ESA, ESTEC, NL-2200 AG Nordwijk, The Netherlands.

[4] Royal Greenwich Observatory, Madingley Road, Cambridge CB3 0EZ, UK.

© American Astronomical Society • Provided by the NASA Astrophysics Data System

1996ApJ...469..554C

with radius; this is not expected if the ionization is purely from the nuclear source because of geometrical dilution of the radiation field, unless the density is decreasing as r^{-2} to compensate. The existing ground-based measurements argue against this latter explanation (Capetti et al. 1995a). The presence of extended UV emission, which they interpreted as free-free emission from hot gas, shocked by the radio ejecta, led them to suggest that the correct explanation of this result was that there is a significant source of local ionization contributing to the ionizing photon budget.

Establishing the relationship between the radio and optical emission-line regions in other Seyfert galaxies is of great importance in order to determine whether conelike (nuclear ionized) or linear (shock-driven) structures are predominant in the NLR. Another important factor is what role the gravitational potential has in determining the disposition of gas in the NLR. Here we present new *HST* emission-line and continuum observations of two further galaxies, Mrk 573 and Mrk 348, with extended radio emission. In addition, we present post-COSTAR observations of Mrk 3 and Mrk 78 (Capetti et al. 1994, 1995a) which were already observed before the COSTAR deployment. In the case of Mrk 78, this reveals considerably more extended structure and also enables us to investigate the ionization structure of its NLR, while the primary purpose of the Mrk 3 observations was to take advantage of the higher quality of the optically corrected *HST* images to analyze the microstructure of its NLR.

In order to investigate the relationship between the structure of the emission line gas and the gravitational potential of the host galaxy, we also obtained *R*-band observations of Mrk 3 and Mrk 78 with the William Herschel Telescope.

Our observations confirm the causal role played by the interaction between the radio ejecta and the ambient gas in the formation of the narrow-line region and its ionization structure.

Details of the observations and data reduction are given in § 2; the results for the individual objects are presented in § 3, and in § 4 we describe the implications for our understanding of the NLR. In § 5 we discuss the morphology of the NLR and its relationship to the large-scale structure of the host galaxy. A summary can be found in § 6. Throughout this paper we adopt $H_0 = 50$ km s^{-1} Mpc^{-1}. With this assumption, at the redshift of Mrk 573, $z = 0.017$, 0.″1 correspond to 49 pc, while for Mrk 348, $z = 0.015$, for Mrk 78, $z = 0.0386$, and for Mrk 3, $z = 0.0133$; this yields 43, 110, and 39 pc, respectively.

2. OBSERVATIONS AND DATA REDUCTION

The four galaxies in this program were observed using the Faint Object Camera (FOC) on board the *Hubble Space Telescope* in the f/96, 512 × 512 mode (Nota et al. 1994); the pixel size is of 0.″014 × 0.″014, and the field of view is about 7″ × 7″. Four different medium-band filters were used (F210M, F372M, F502M, and F550M) with exposure times ranging from 600 to 2100 s (see Table 1 for the *HST* observations log). The filters were selected to include the emission from the [O II] λ3727 and [O III] λλ4959,5007 lines, the adjacent optical continuum, and the UV continuum. The FOC data have been reduced following the standard procedure for the FOC data (see, e.g., Capetti et al. 1995a) which includes corrections for the geometric distortion, flat-field, linearity, as well as background removal and continuum subtraction.

TABLE 1

OBSERVATIONS LOG

Date	*HST* Root Name	Filter	Exposure Time (s)
	Mrk 5736		
1994 Feb 9.....	X2580505T	F210M	596
	X2580502T	F372M	1072
	X2580503T	F502M	896
	X2580504T	F550M	1301
	Mrk 348		
1994 Feb 17	X2580403T	F210M	891
	X2580401T	F502M	2128
	X2580402T	F550M	1796
	Mrk 78		
1994 Mar 19.....	X2580305T	F210M	596
	X2580302T	F372M	896
	X2580303T	F502M	801
	X2580304T	F550M	1196
	Mrk 3		
1994 Mar 20.....	X2580105T	F210M	596
	X2580102T	F372M	896
	X2580103T	F502M	750
	X2580104T	F550M	1196

Since the narrow-line region of Mrk 573 is more extended than the FOC field of view, further observations were taken with the Wide Field Planetary Camera 2 (WFPC2). The Planetary Camera has a pixel size of 0.″046 and covers a field of view of 37″ × 37″. The wide filters F569W, F675W, and F814W were used to map the [O III], Hα, and continuum emission, respectively. Two exposures of duration 600 s were obtained for each filter. The observations were processed through the PODPS (Post Observations Data Processing System) pipeline for bias removal and flat-fielding. Each pair of exposures was combined to remove cosmic rays.

In order to derive pure emission-line images, the observations in the continuum have been suitably scaled and subtracted from each of the on-band images.

Flux calibration was obtained using the internal calibrations of both the FOC and WFPC2 and is accurate to within ±5%. The integrated NLR line fluxes measured from our images are always within 20% of the ground-based measurements by Koski (1978).

Broadband Johnson *R* images of Mrk 3 and Mrk 78 were obtained at the auxiliary focus of the William Herschel Telescope using a 1024 × 1024 Tektronix array on 1993 December 13. The pixel size was 0.″11, and the exposure times were of 800 and 500 s with seeing of 1.″5 and 1.″0 for Mrk 3 and Mrk 78, respectively.

3. RESULTS

3.1. *Mrk 573*

3.1.1. *The Emission-Line Structure of Mrk 573*

The [O III], [O II], and Hα emission-line images of Mrk 573 are presented in Figures 1*a*, 1*b*, and 2 (Plates 21–22), respectively. These three images are remarkably similar both in the large- and small-scale structure.

On both the northwest and southeast sides, the large-scale emission-line structure is dominated by two spectacu-

© American Astronomical Society • Provided by the NASA Astrophysics Data System

1996ApJ...469..554C

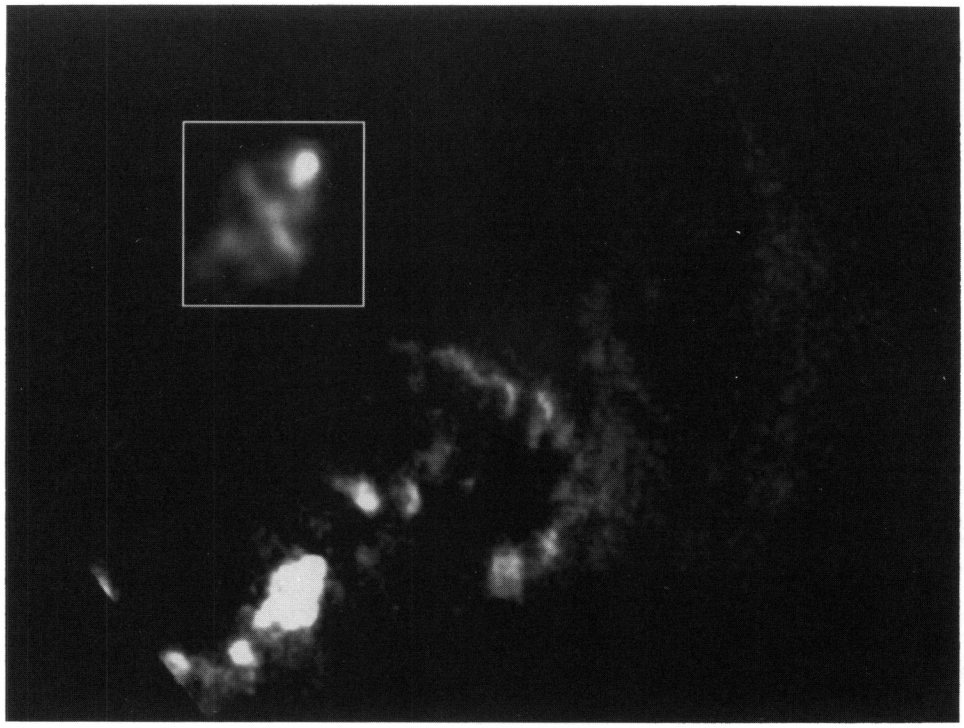

FIG. 1*a*

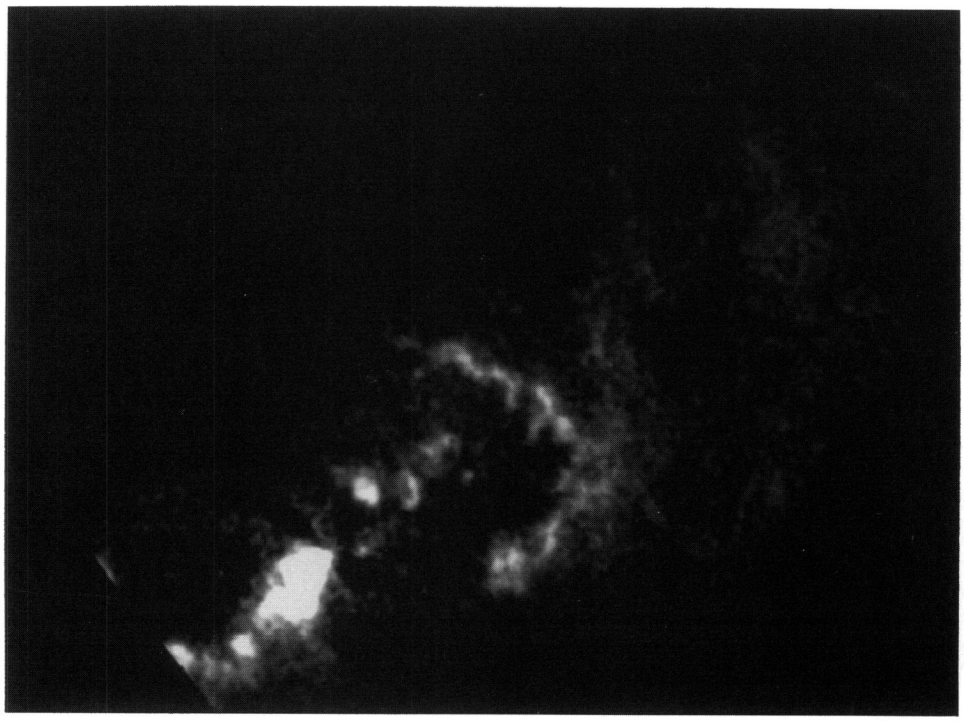

FIG. 1*b*

FIG. 1.—(*a*) [O III] emission-line image of Mrk 573. The inset shows the bright knot with a different contrast to evidence its fine-scale structure. (*b*) [O II] emission-line image of Mrk 573. The field of view for these images is 6.″6 × 4.″9.

© American Astronomical Society • Provided by the NASA Astrophysics Data System

1996ApJ...469..554C

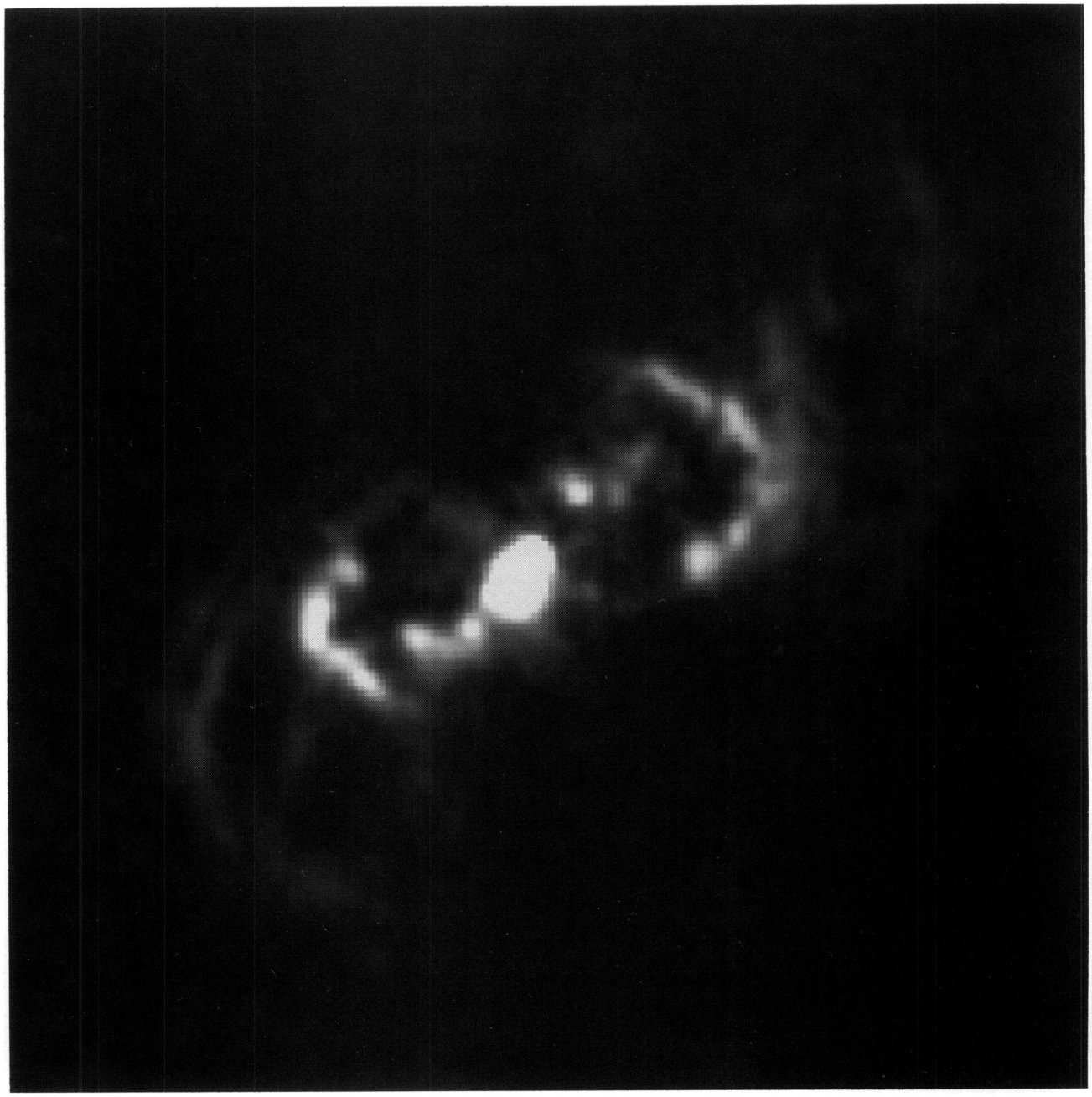

FIG. 2.—Hα emission-line image of Mrk 573 obtained with the WFPC2. The field of view for these images is 8.″7 × 8.″7

CAPETTI et al. (see 469, 555)

© American Astronomical Society • Provided by the NASA Astrophysics Data System

1996ApJ...469..554C

lar narrow arcs, which are located at ~1".5 from the nucleus and span from P.A. = 80 to P.A. = 160. Both arcs show significant corrugations and are broken into alternating dark and bright regions. In the Hα image (Fig. 2), these arcs appear to be linked to the central region by two weaker S-shaped emission features, giving this complex the overall appearance of a double bubble.

Fainter and more diffuse arcs are seen at larger radii on both sides of the NLR at a distance as large as 4" (~2 kpc) from the nucleus and cover approximately the same range in position angles as the inner arcs.

The detailed structure of its central region is shown in finer detail in the inset to Figure 1*a*, in which it is apparent that the brightest knot of Figure 1 is itself resolved into a series of smaller knots. Its overall appearance is very similar to that of the "knot B" region in NGC 1068 (Macchetto et al. 1994).

The similarity between the structure seen in the different emission lines is confirmed quantitatively by Figure 3. Individual details in the radial surface brightness profiles reproduce well in [O III], [O II], and Hα. The [O III]/[O II] ratio has only been measured on the western side of the NLR because the eastern side is out of the field of view of the FOC. The emission-line ratios [O III]/[O II] and [O III]/Hα are essentially constant within the innermost 2" ([O III]/[O II] ~ 3 and [O III]/Hα ~ 1.5), and they increase by ~30% on the outer filaments where [O III]/[O II] ~ 4 and [O III]/Hα ~ 2.

3.1.2. *The Continuum Structure of Mrk 573*

The large-scale continuum structure of Mrk 573 as seen through the F814W filter is shown in Figure 4. A bar with a radius of ~10" (4.9 kpc) at position angle ~0° is superimposed on an elliptical bulge. Figures 5*a*–5*d* present the results obtained from fitting elliptical isophotes to this image. Plotted in each of the panels are the luminosity profile, position angle, ellipticity, and B4 parameter. The effects of the presence of the large-scale bar are clear in each of these plots. There is a marked twist in the major axis of the isophotes at a radius of 5" (2.4 kpc) interior to which their major axes become nearly perpendicular to the large scale bar. This switch in orientation is accompanied by large changes in ellipticity and B4 parameter, which measures the degree of "boxiness" of the isophotes, and it occurs on the same physical scale of the NLR. However, the major axis of the inner structure is misaligned by the radio axis by ~35°.

The F550M off-band filter (Fig. 6*a* [Pl. 23]) shows a bright central knot which is fully resolved, with an FWHM of ~0".1, which corresponds to the bright knot of line emission seen in the inset of Figure 1*a*. This is embedded in an extended lower surface brightness elliptical halo oriented at P.A. = +100, which is well aligned with the bulge of Mrk 573 (Fig. 4). Close to the bright knot, there is a narrow and twisted absorption feature which runs across the minor axis of the nuclear region and is approximately perpendicular to

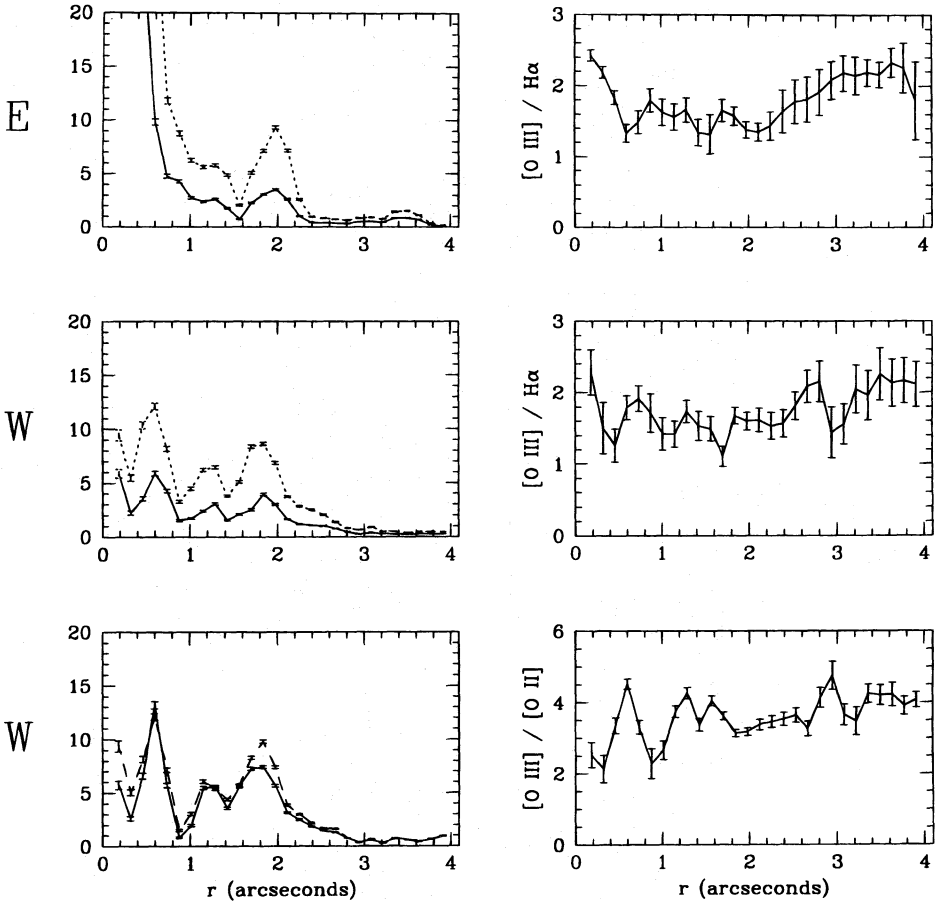

FIG. 3.—*Left panels*: composition of the radial brightness profiles of [O III] (*solid line*), [O II] (*dashed line*), and Hα (*dotted line*) measured on the two sides of the nucleus separately; the [O II] FOC image covers only the west side of the NLR. Fluxes are given in arbitrary units. *Right panels*: the corresponding line ratios.

© American Astronomical Society • Provided by the NASA Astrophysics Data System

1996ApJ...469..554C

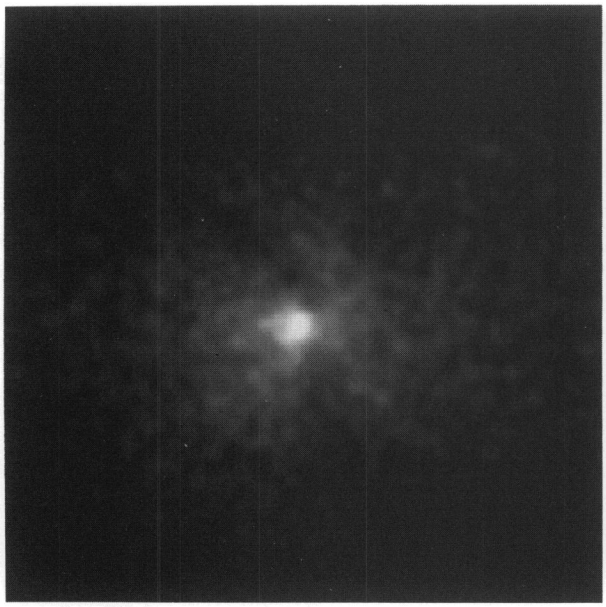

FIG. 6a

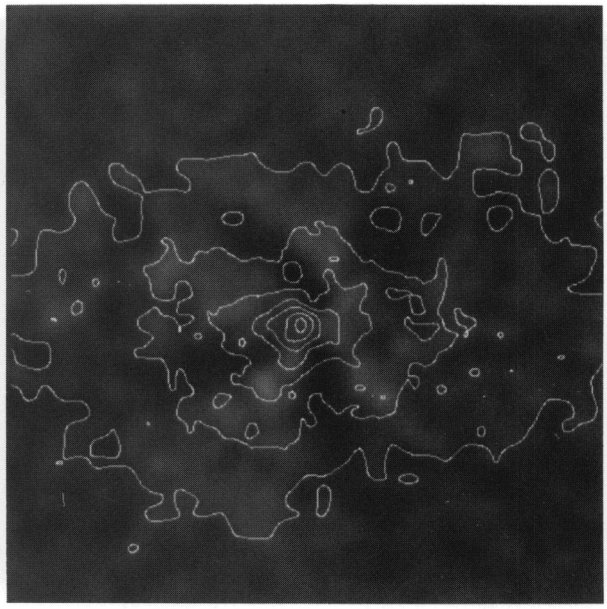

FIG. 6b

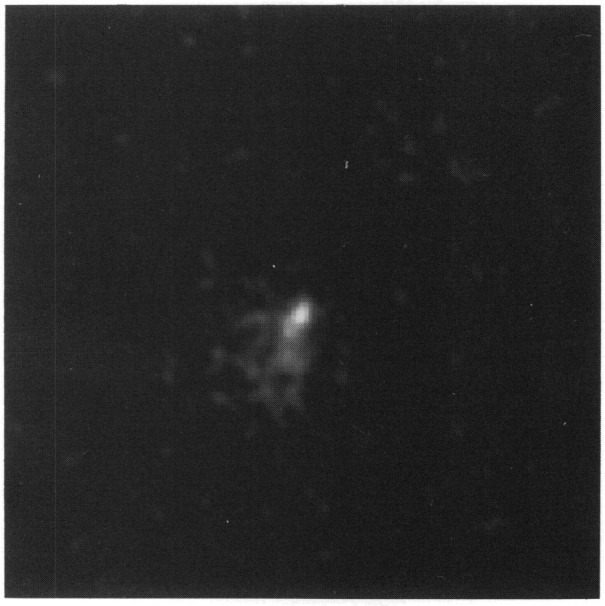

FIG. 6c

FIG. 6.—(*a*) Visual continuum image (F550M filter) of Mrk 573; (*b*) residual after the subtraction of an elliptical model from the visual continuum image with superposed the contour plot of the original image; (*c*) ultraviolet continuum image (F210M filter) of Mrk 573. The field of view for these images is 2″ × 2″. All the images are shown with north to the top and east to the left.

© American Astronomical Society • Provided by the NASA Astrophysics Data System

1996ApJ...469..554C

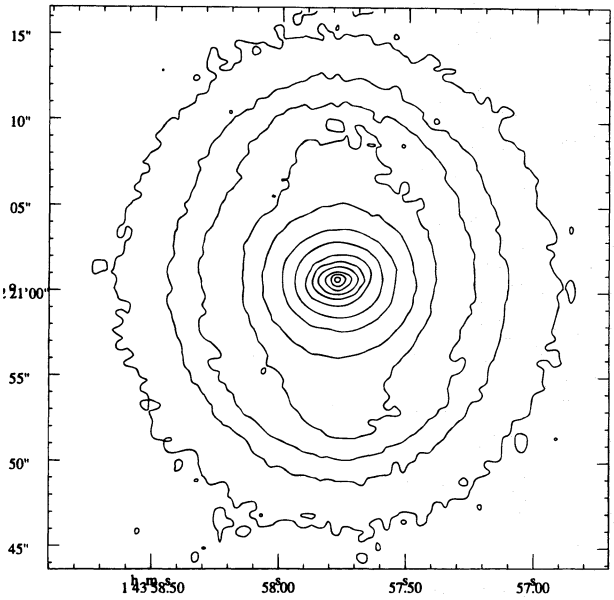

FIG. 4.—*HST* contour image of Mrk 573 obtained through the F814W filter. The field of view is 33″ × 33″. Note the bar extending along position angle ~0°.

the major axis of the NLR and the radio extended emission (P.A. ~ 55°; Wilson & Ulvestad 1983). The F210M UV image (Fig. 6*c*) shows a marginally resolved, FWHM ~ 0.″05, knot coincident with that seen in the optical continuum. There is also a weak extension from the knot toward the south-east for ~0.″5 which shares the elongated morphology seen in the emission line (Fig. 1*a*, inset). Unfortunately, the signal-to-noise ratio of this image is not good enough to tell if there is lower surface brightness UV continuum associated with the arclike structures.

Much of the continuum at 5500 Å is due to starlight. In order to study the inner structure of the galaxy in more detail, we modeled the stellar component by fitting elliptical isophotes to the image. The result of subtracting this model from the F550M image is shown gray scale in Figure 6*b*; superimposed is a contour map of the original image. It clearly shows the dust lane, which spans ~1″ (500 pc) and has a width of ~0.″1 (50 pc); it is significantly warped, with a change in position angle larger than ~30°. The observed absorption corresponds to $A_V \sim 0.5$. The bright knot is located ~0.″1 westward of the dust lane. This displacement suggests that the dust lane is tilted so that the south west side of Mrk 573 lies foreground to it.

3.2. *Mrk 348*

Figure 7*a* (Plate 24) shows the inner structure of the [O III] image of Mrk 348. The line emission is confined to a linear structure, 0.″45 in size, oriented at position angle ~155 and is split into two distinct regions by a prominent absorption feature. The northern section is highly collimated and jetlike, extending to a radius of ~0.″2 at which point it suddenly bends and terminates in an equally narrow and nearly orthogonally orientated feature. In contrast, the morphology of the southern component is rad-

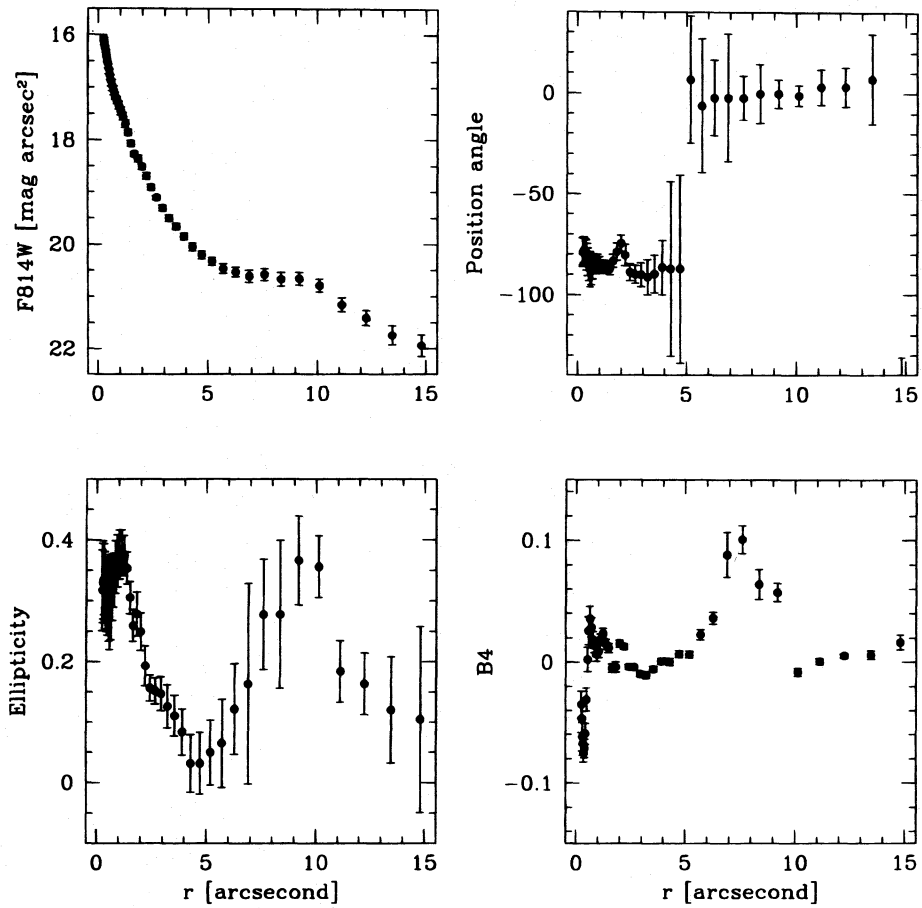

FIG. 5.—Results obtained by fitting elliptical isophotes to the F814W image of Mrk 573. Plotted in each of the panels are the luminosity profile, position angle, ellipticity, and B4 parameter.

© American Astronomical Society • Provided by the NASA Astrophysics Data System

1996ApJ...469..554C

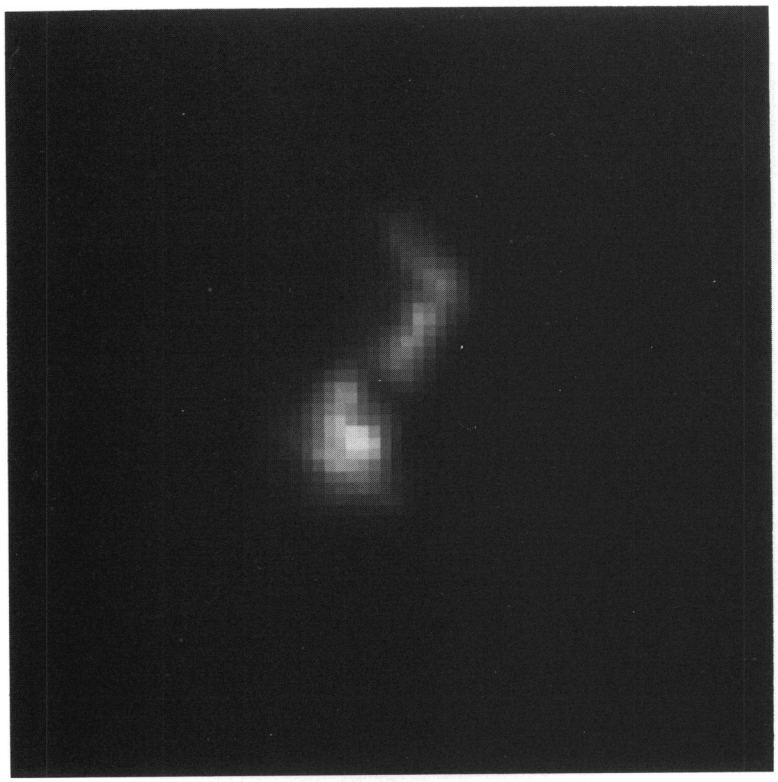

FIG. 7*a*

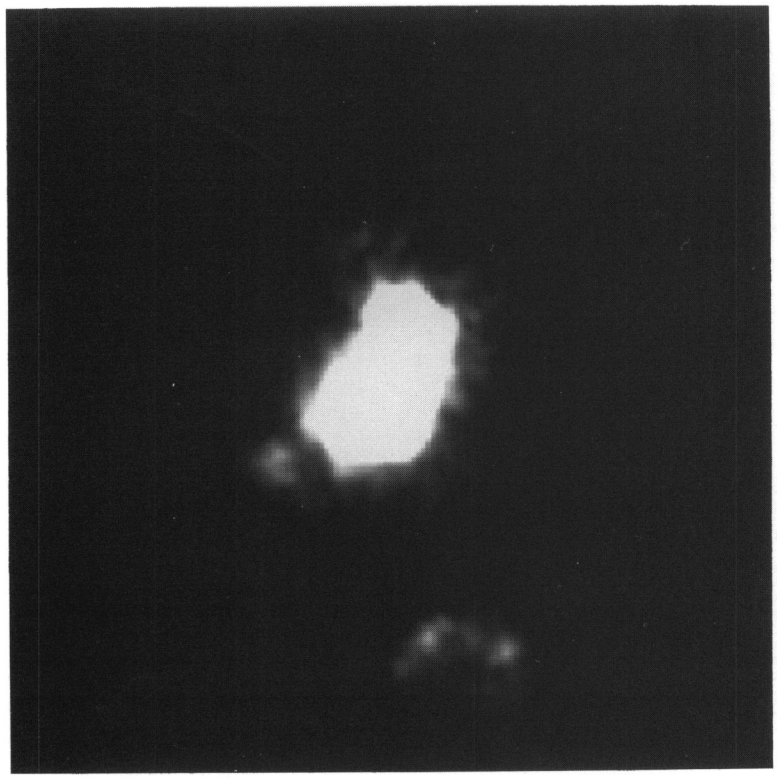

FIG. 7*b*

FIG. 7.—[O III] emission-line image of Mrk 348 with a field of view of (*a*) 1″ × 1″ and (*b*) 2.″2 × 2.″2

© American Astronomical Society • Provided by the NASA Astrophysics Data System

1996ApJ...469..554C

ically different, appearing as an arclike lobe on which a bright knot is superimposed.

Outside this central region, two much weaker emission line knots are seen (see Fig. 7*b*). The first lies at a radius of ~0.″5 along the same axis as the inner structure and shows no evidence of substructure at this resolution. The second, located 0.″9 southwest of the nucleus, shows a shell-like morphology, brighter on the northern than on the southern side, and it is resolved with a diameter of ~0.″36. Its integrated flux contributes ~4% of the total line emission.

The visual continuum image (Fig. 8*a* [Pl. 25]) shows a very similar morphology to that of [O III] in the bright central region; again with a linear northern section, broken from a more bloblike southern section by the dust lane. As in Mrk 573, this central structure is superposed on a diffuse plateau of continuum (Fig. 8*b*), which is presumably stellar in origin. There is no evidence for a continuum counterpart to the outer emission-line shell we discussed above.

3.3. *Mrk 78*

3.3.1. *The Emission-Line Structure of Mrk 78*

Pre-COSTAR HST [O III] observations were presented by Capetti et al. (1994). Their [O III] image showed a biconical NLR approximately along P.A. ~ 67° with a resolved 0.″8 in extent, obscuring region close to the center of the cone.

The new [O III] and [O II] images (Figs. 9*a* and 9*b* [Pl. 26]) show that NLR is substantially more extended at low surface brightness and has a double-lobed structure. The eastern lobe is relatively bright and compact eastern lobe 0.″9 × 1.″1, and its morphology still retains a vaguely conical appearance. The western lobe is not only fainter but takes the form of a highly structured diffuse shell whose size, 1.″5 × 2.″3, is nearly twice that of the eastern lobe. The outer boundary has relatively sharp edges and a complex small-scale corrugated structure, very reminiscent of that described for Mrk 573. The broad absorption region seen by Capetti et al. (1994) is punctuated with a series of emission knots, but a deep and narrow absorption feature still marks the intersection of the two lobes.

The addition of the [O II] image also allows us to investigate the ionization structure on the NLR (fig. 9*c*). The eastern lobe shows high ionization ([O III] λ5007/[O II] λ3727 ~ 2.9), while the ionization structure of the western lobe is somewhat different since it only shows high ionization close to the nucleus. Throughout the outer low-ionization region of the western shell, [O III] λ5007/[O II] λ3727 ~ 1.4.

The value we obtained for the higher ionization regions is comparable to that seen throughout the western lobe of Mrk 573 but somewhat lower than that seen in the jet of Mrk 3 (~7; Capetti et al. 1995a and § 3.4).

3.3.2. *The Continuum Structure of Mrk 78*

The WHT *R*-band image of Mrk 78 is shown in Figure 10. Figures 11*a*–11*b* present the results obtained by fitting elliptical isophotes to this image. In the outer regions, the position of the major axis is 145°, whereas in the central region there is a small swing of position angle, ~10°, to higher P.A., but this is far less dramatic than that seen in Mrk 573. Note, however, that a double-bar structure with similar linear dimensions to that of Mrk 573 would not have been detected in our ground-based observations due to the distance of Mrk 78.

The FOC F550M image smoothed to 0.″25 resolution (Fig. 12) reveals that the continuum structure in the innermost 4″ is very elongated and oriented along P.A. = 75°. At

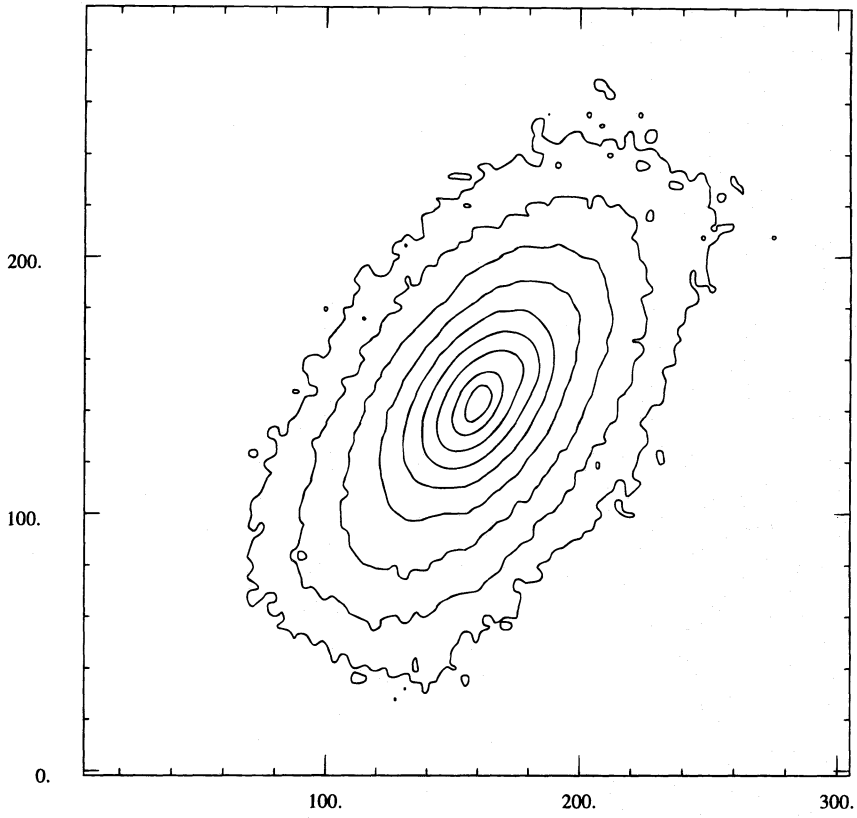

FIG. 10.—WHT *R*-band contour image of Mrk 78. The field of view is 33″ × 33″.

© American Astronomical Society • Provided by the NASA Astrophysics Data System

1996ApJ...469..554C

PLATE 25

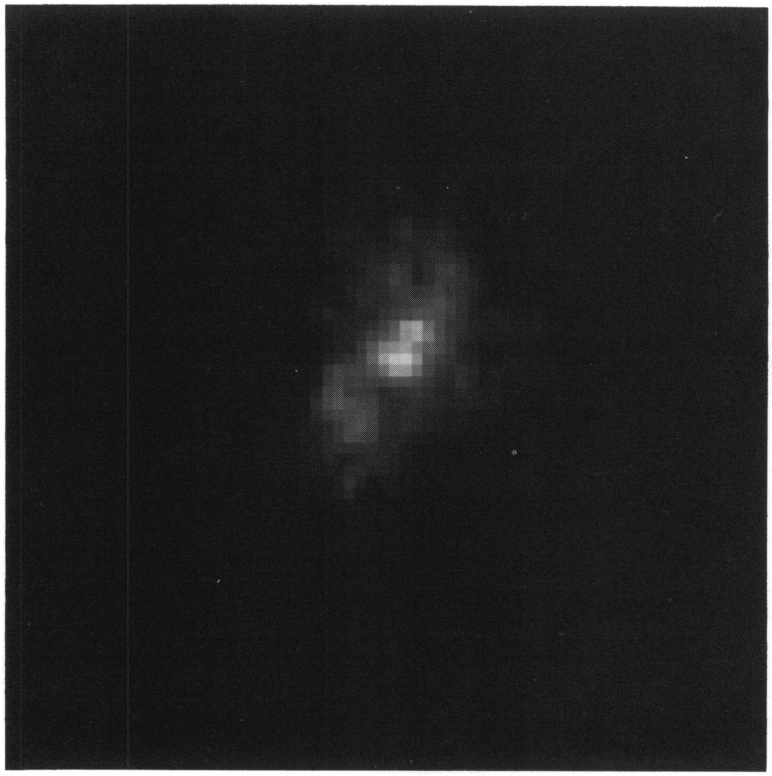

FIG. 8*a*

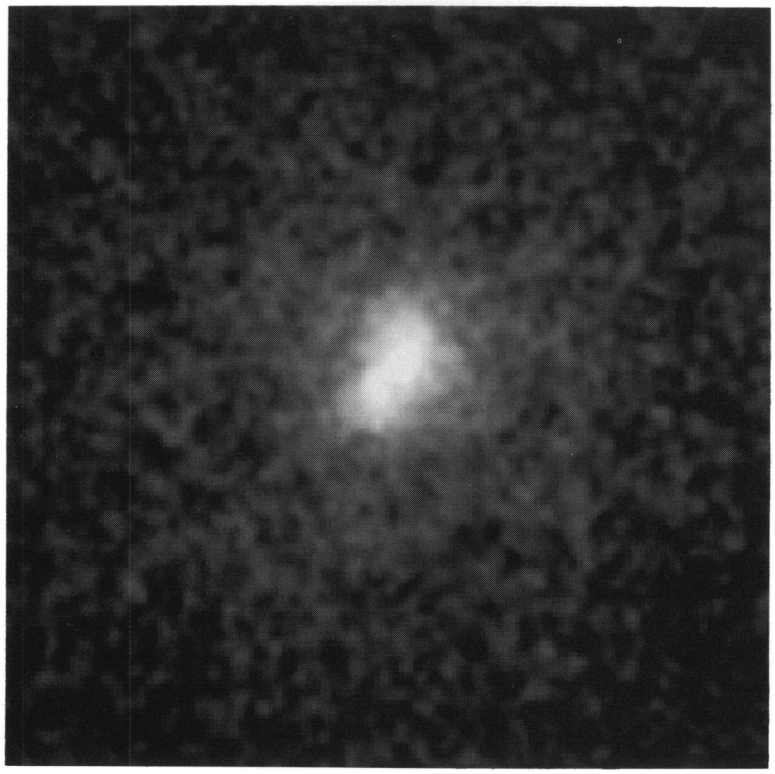

FIG. 8*b*

FIG. 8.—Visual continuum image of Mrk 348 with a field of view of (*a*) 1″ × 1″ and (*b*) 2.″2 × 2.″2

© American Astronomical Society • Provided by the NASA Astrophysics Data System

1996ApJ...469..554C

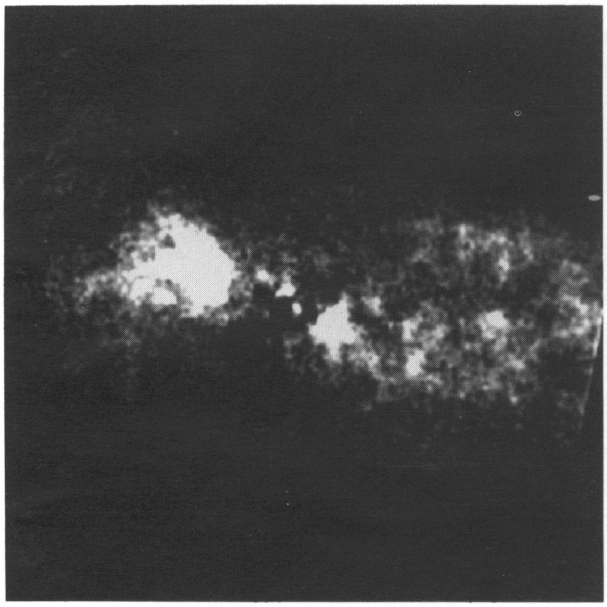

FIG. 9a

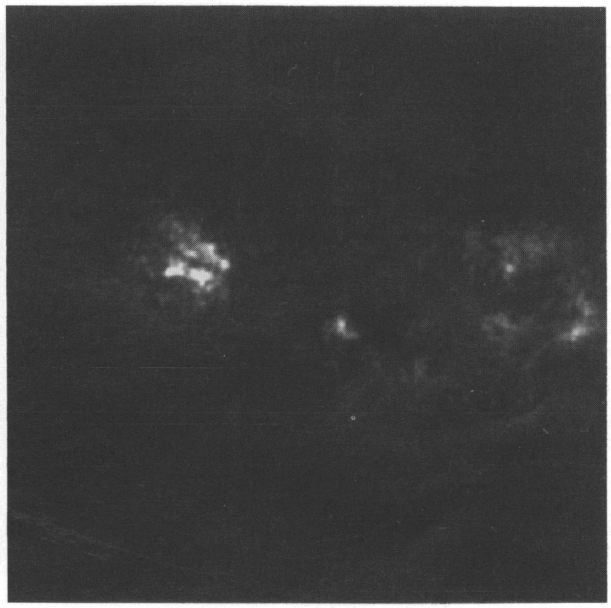

FIG. 9b

FIG. 9c

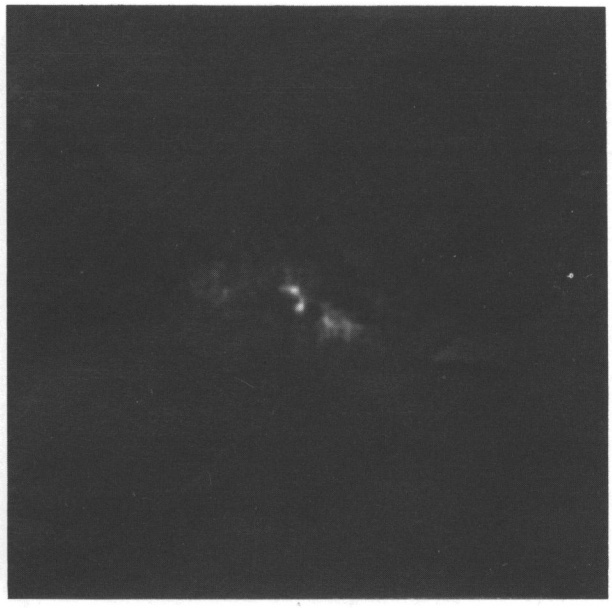

FIG. 9d

FIG. 9.—(*a*) [O III] and (*b*) [O II] emission-line images of Mrk 78. The [O III]/[O II] ratio is shown in (*c*), and the optical continuum image is shown in (*d*). The field of view is 5″ × 5″.

© American Astronomical Society • Provided by the NASA Astrophysics Data System

1996ApJ...469..554C

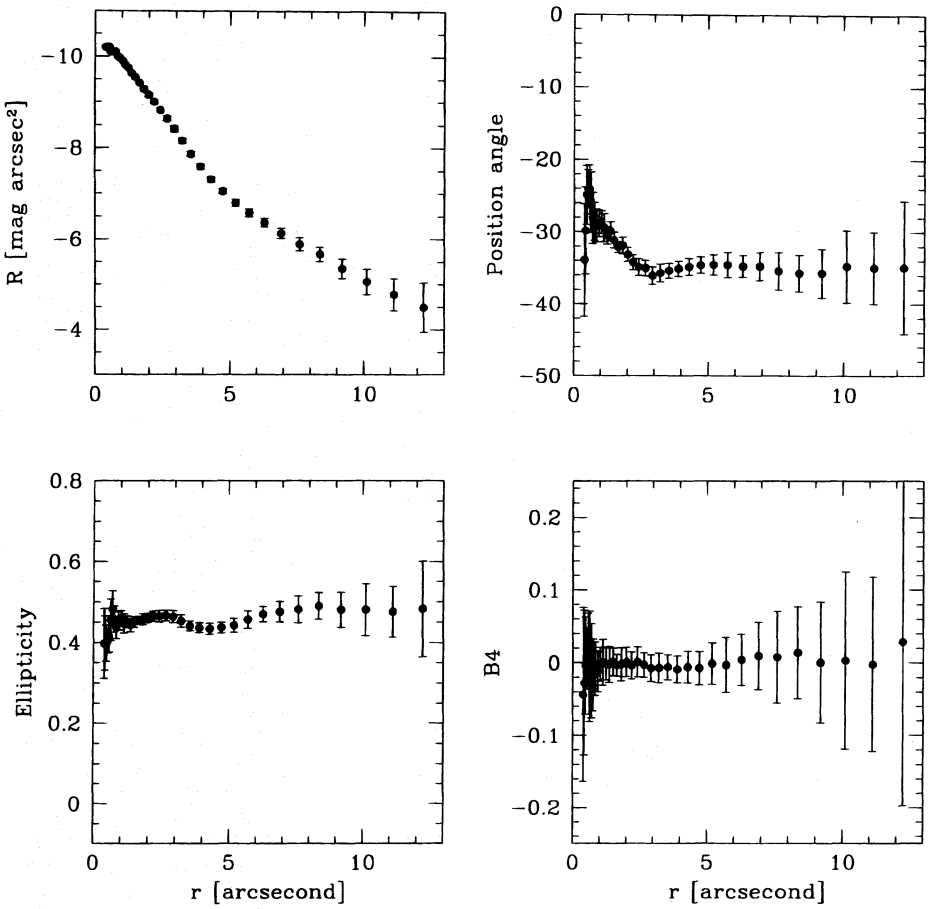

FIG. 11.—Results obtained by fitting elliptical isophotes to the WHT *R*-band image of Mrk 78. Plotted in each of the panels are the luminosity profile, position angle, ellipticity, and B4 parameter.

full resolution (Fig. 9*d*), this image shows two diffuse continuum patches cospatial with the high-excitation regions of the emission-line lobes. A pair of bright compact knots, separated by 0.″15, stand out prominently in the central dust lane which splits the two line emission lobes.

No UV emission is detected at our detection limit of 1.1×10^{-15} ergs s^{-1} Å^{-1} arcsec^{-2}.

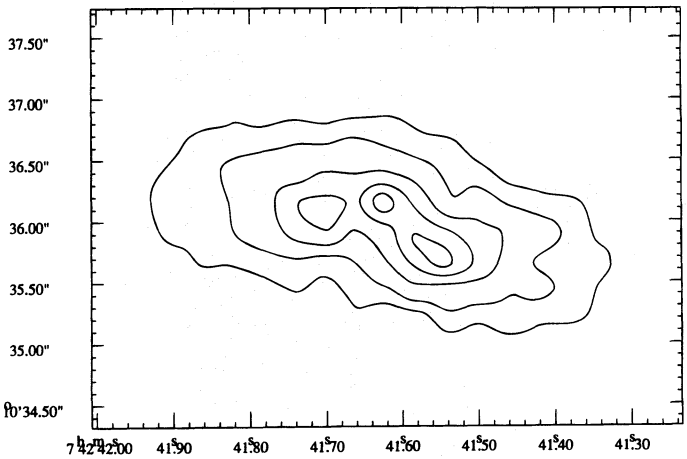

FIG. 12.—*HST* visual continuum image of Mrk 78 at 0.″25 resolution. The field of view is 4.″8 × 3.″4.

3.4. *Mrk 3*

The properties of the NLR of Mrk 3 have been discussed at length in Capetti et al. (1995a). Here we present the COSTAR-corrected images for this galaxy in the [O III] and [O II] emission lines (Fig. 13 [Pl. 27]) and the visual continuum (Fig. 14).

Overall, the emission-line images are reassuringly similar to the deconvolved pre-COSTAR data, and so they will only be discussed briefly. They do, however, show considerably more fine structure, particularly in the diffuse region at the Western end of the S, coincident with the radio hot spot, which is now clearly composed of a whole series of sheets or filaments. The individual knots in the main part in the emission-line bar also appear to be filamentary in nature; this detail was lost in the pre-COSTAR data. Finally, we note that the narrow absorption lane perpendicular to the NLR, which we believe hides the nucleus, is now very evident. This is important because in the original data it was not clear that this was not an artifact of deconvolution, which tends to clump the emission into discrete knots.

The WHT *R*-band image of Mrk 3 is shown in Figure 14. Figures 15*a*–15*d* present the results obtained by fitting elliptial isophotes to this image. The isophotes show clear departures from ellipticity over the whole galaxy as illustrated by the behavior of the B4 parameter; the ellipticity also decreases from ~0.3 to 0.1 in the innermost regions. Subtracting an elliptical galaxy model from the Mrk 3

© American Astronomical Society • Provided by the NASA Astrophysics Data System

1996ApJ...469..554C

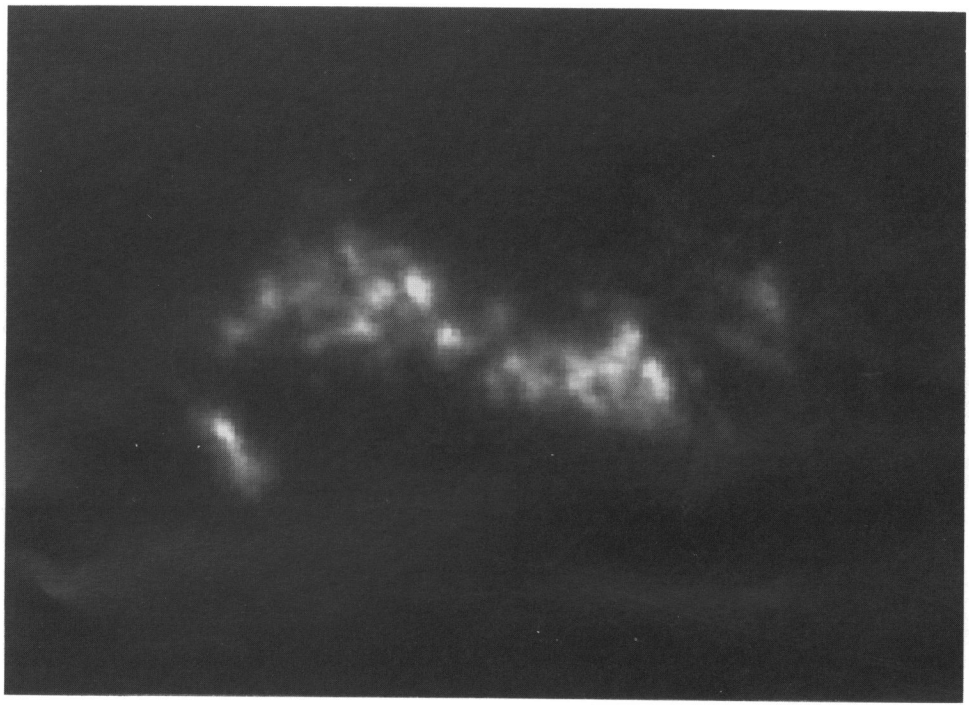

FIG. 13*a*

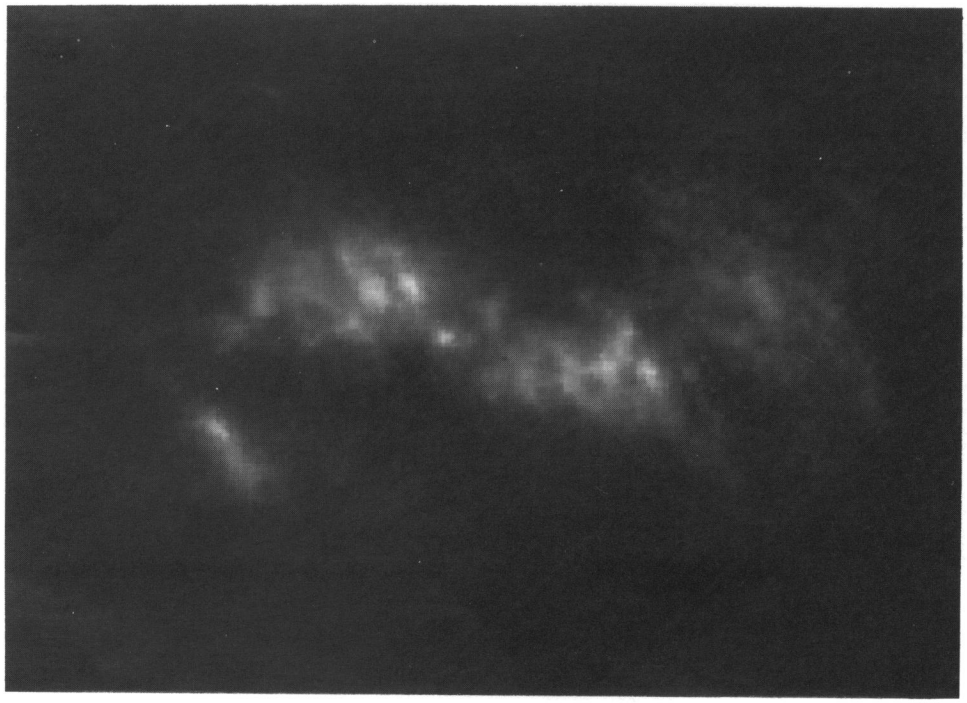

FIG. 13*b*

FIG. 13.—(*a*) [O III] and (*b*) [O II] emission-line images of Mrk 3. The field of view is 3.″0 × 2.″2.

© American Astronomical Society • Provided by the NASA Astrophysics Data System

1996ApJ...469..554C

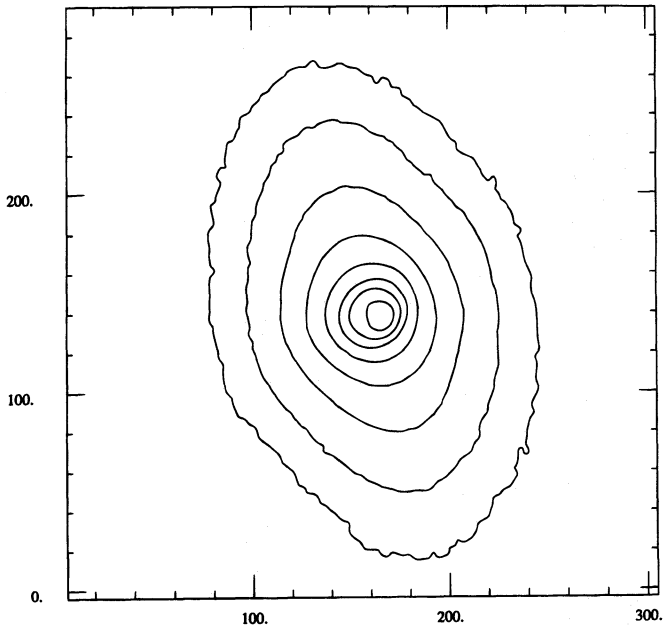

FIG. 14.—WHT *R*-band contour image of Mrk 3. The field of view is 33″ × 33″.

image shows that the residuals are concentrated mainly along the minor axis of the bulge. Within a radius of ~3″, the position angle changes from the position angle of the large-scale emission (P.A. ~ 20°) to significantly lower values, but the exact behavior is hard to ascertain because of the limited resolution of the ground-based data. A much clearer understanding of what is happening in this central region can be reached using the *HST* images. The *HST* continuum image (Fig. 16 [Pl. 28]), which is essentially line free, confirms the existence of the small-scale continuum bar (Fig. 16*a*) oriented at P.A. = +70°, nearly perpendicular to the bulge, which we believe is the origin of the large twist seen in the ground-based data. In the high-contrast figure (Fig. 16*b*), the relationship between this inner bar and the outer bulge is clearly visible.

In the original *HST* continuum image presented by Capetti et al. (1995a), there was significant contamination from emission lines which had to be removed by synthetic modeling; the new data demonstrate convincingly that the bar is not a consequence of residual line contamination. The new image also shows that the southern edge of the bar is delineated by a broad linear dust lane, as is often seen on the leading edge of bars in both computer simulations and real barred galaxies.

4. THE RELATIONSHIP BETWEEN THE RADIO AND NLR STRUCTURE

In Figure 17 (Plates 29–32) we present the emission-line images for all four galaxies with the corresponding radio maps overlain as contours. We have aligned the radio and *HST* images of Mrk 573, Mrk 348, and Mrk 3 by assuming that the radio core is located behind their nuclear dust lanes. In the case of Mrk 78, the registration is less clear

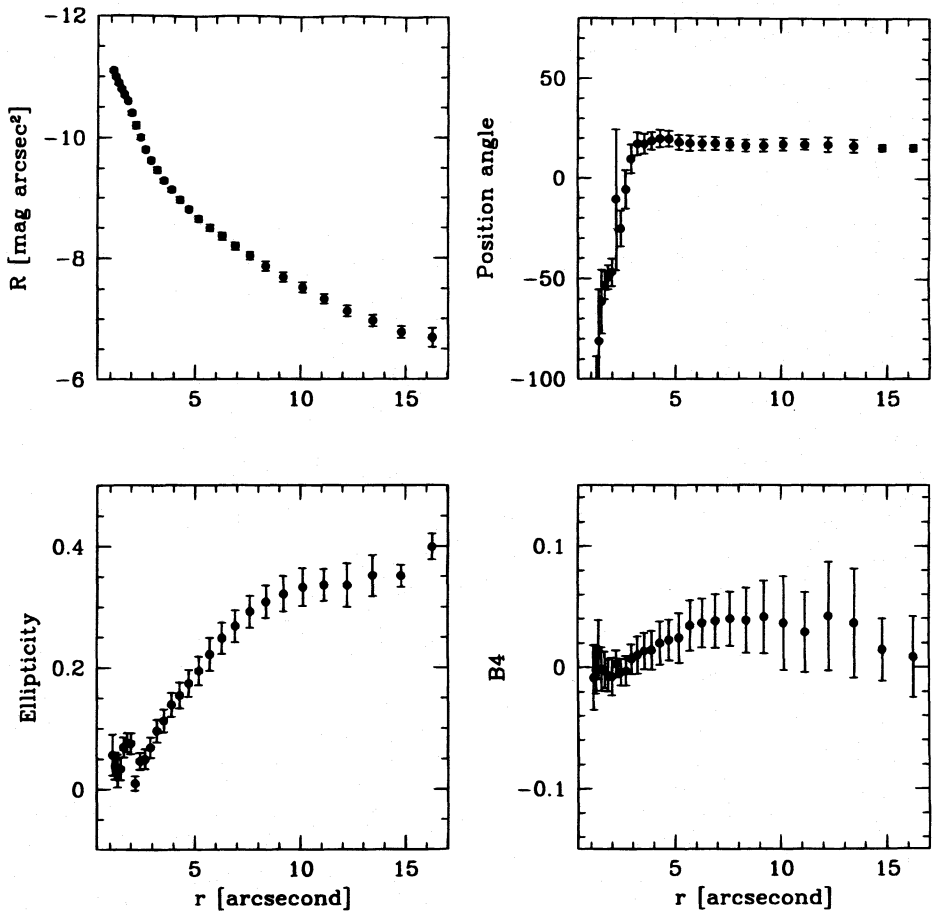

FIG. 15.—Results obtained fitting elliptical isophotes to the WHT *R*-band image of Mrk 3. Plotted in each of the panels are the luminosity profile, position angle, ellipticity, and B4 parameter.

© American Astronomical Society • Provided by the NASA Astrophysics Data System

1996ApJ...469..554C

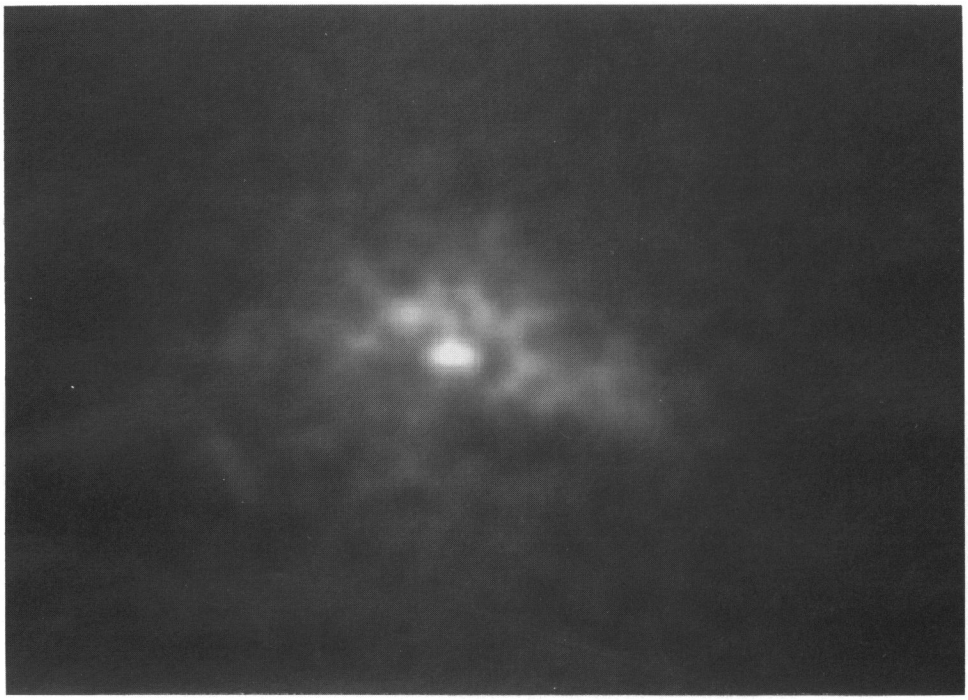

FIG. 16*a*

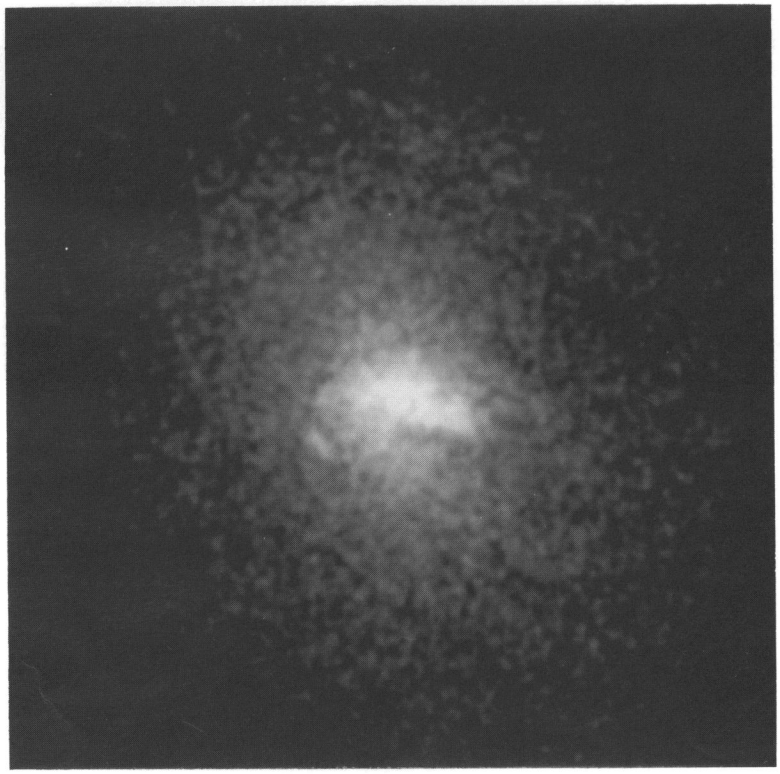

FIG. 16*b*

FIG. 16.—(*a*) *HST* visual continuum image of Mrk 3 shown with a field of view of (*a*) 3.″0 × 2.″2

© American Astronomical Society • Provided by the NASA Astrophysics Data System

1996ApJ...469..554C

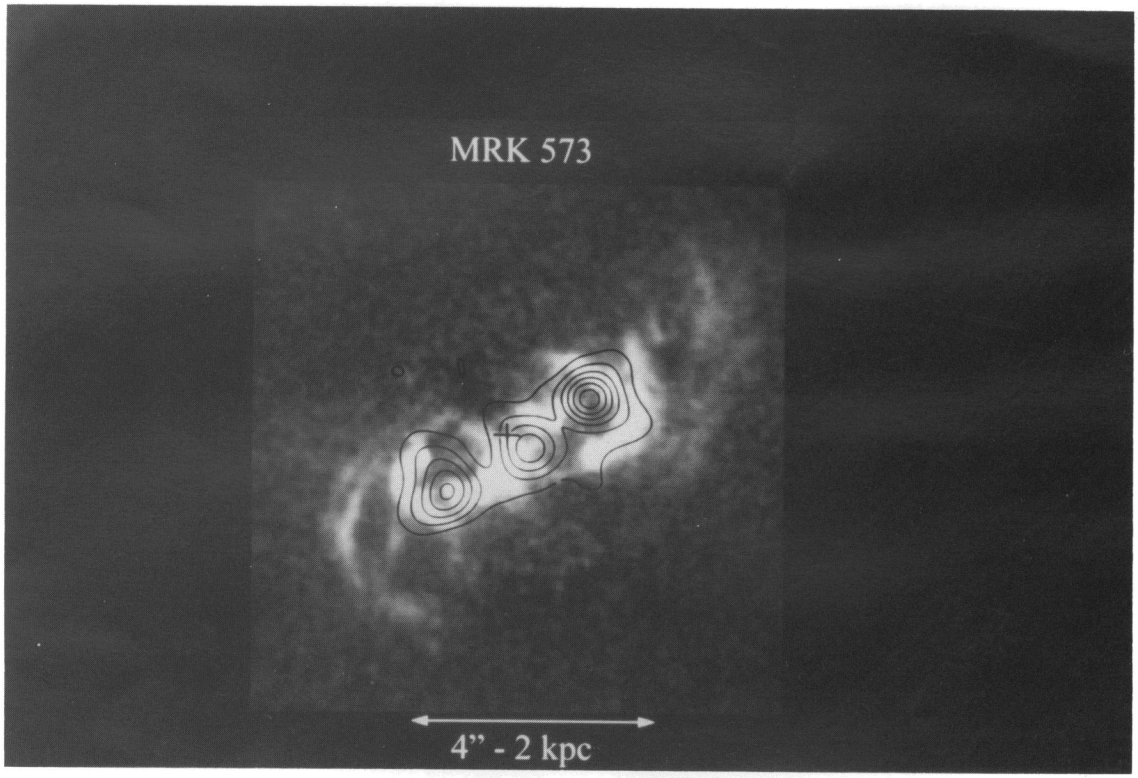

FIG. 17*a*

FIG. 17.—Emission-line images with the radio contour images of (a) Mrk 573, (*b*) Mrk 348, (*c*) Mrk 78, and (*d*) Mrk 3 superposed.

CAPETTI et al. (see 469, 560)

© American Astronomical Society • Provided by the NASA Astrophysics Data System

1996ApJ...469..554C

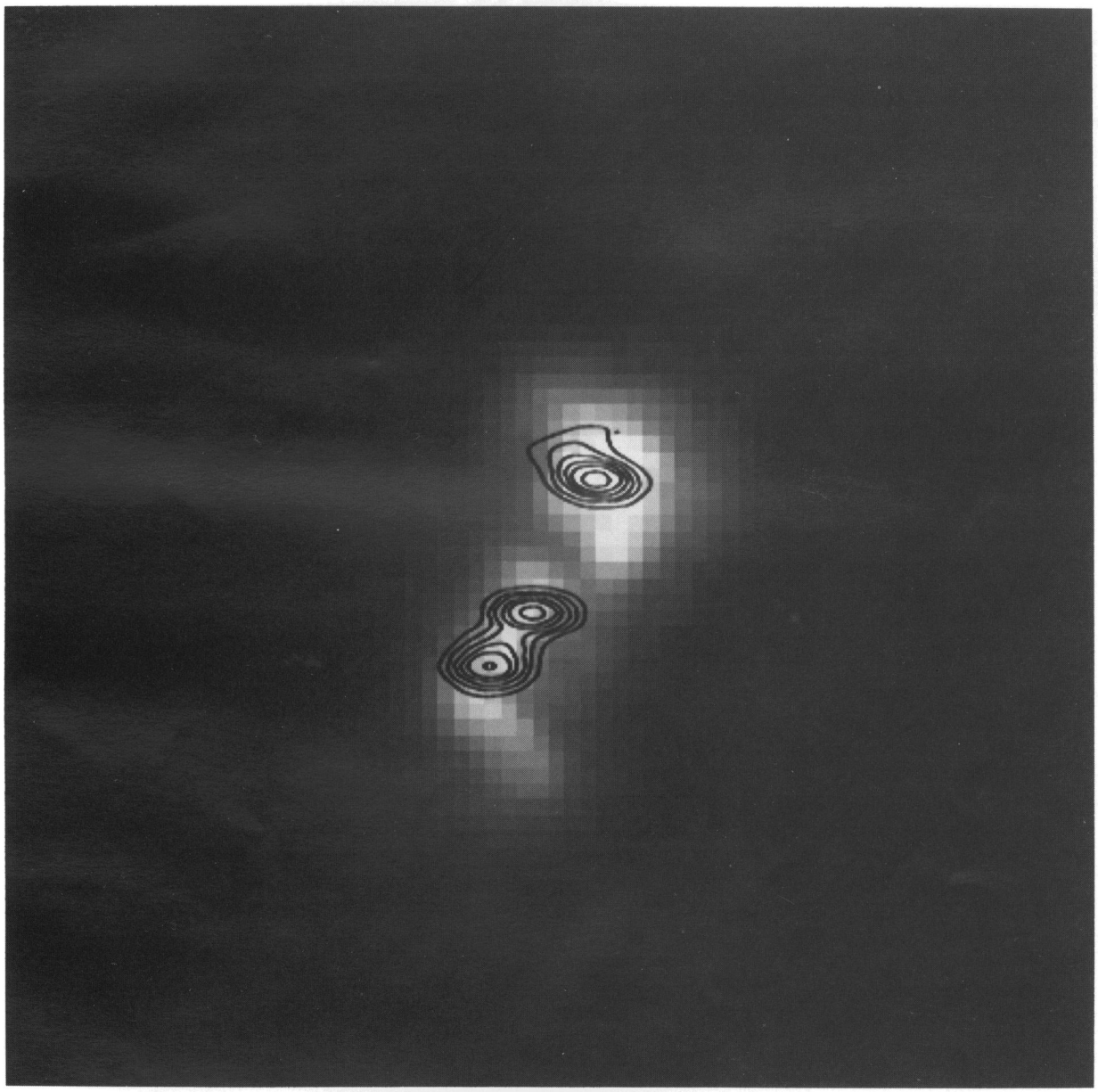

FIG. 17*b*

CAPETTI et al. (see 469, 560)

© American Astronomical Society • Provided by the NASA Astrophysics Data System

1996ApJ...469..554C

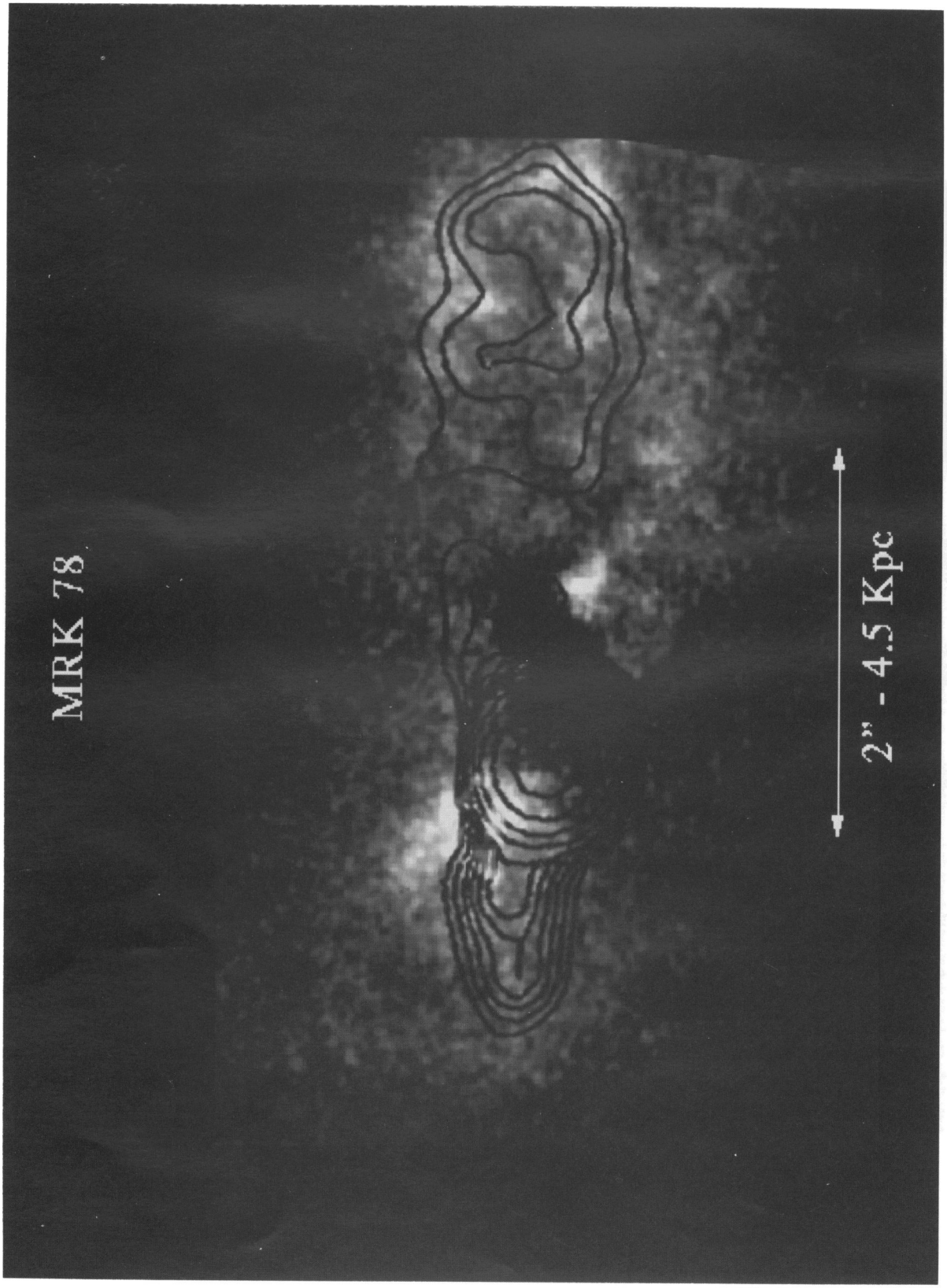

FIG. 17c

© American Astronomical Society • Provided by the NASA Astrophysics Data System

1996ApJ...469..554C

FIG. 17*d*

CAPETTI et al. (see 469, 560)

© American Astronomical Society • Provided by the NASA Astrophysics Data System

1996ApJ...469..554C

because of the complexity of structure of the nuclear region. Therefore, we have used the similarity of the radio and optical morphologies to align the radio and *HST* images.

The 3.6 cm VLA radio image of Mrk 573 (Wilson & Ulvestad 1983) shows a triple structure. The central component is located only 0".2 from the position of the optical nucleus as measured by Clements (1981), and we assume it to be the radio core. The two radio lobes are positioned at P.A. = 135° and 138° at a distance of 1".2 and 1".7 for the northwest and southeast lobe, respectively.

The 5 GHz VLBI radio contour image of Mrk 348 (Pedlar & De Bruyn 1995, private communication) at 50 mas resolution shows a quasi-linear structure, dominated by three compact components 0".25 in size and oriented at P.A. = 168°. The central component is probably the radio core, having an inverted radio spectrum (Unger et al. 1986).

The 2 cm VLA radio image of Mrk 78 (Pedlar et al. 1989) at 0".15 resolution also shows a triple structure, dominated by a bright core. The radio structure on the two opposite sides of the nucleus is quite different; while the east side has jetlike morphology, on the west side there is a more diffuse radiolobe.

For Mrk 3, as in Capetti et al. (1995a), we used the MERLIN image by Kukula et al. (1993).

Inspecting Figure 17, it is clear that in all cases the physical structure of the NLR is closely related to the radio emission and its morphology is dominated by the interaction with the radio ejecta. Furthermore, it appears that the NLR takes a different form depending on the structure of the radio emission. Whenever radio lobes are observed, they are accompanied by shell-like emission-line structures. In the case of Mrk 573, the emission-line structure takes the form of a series of bow shocks with the apex of the brightest eastern and western bows being located at the position of the corresponding radio lobe. A very similar structure is seen on the western lobe of Mrk 78 and on the southeastern lobe of Mrk 348. In Mrk 3, the emission was associated with the western hotspot is also diffuse, but more filamentary than shell-like. This difference might arise because the hot spot of Mrk 3 is more compact than the lobes seen in the other two galaxies (A. Pedlar, 1995, private communication).

A rather different impression of the relationship between the emission-line gas and the radio structure is apparent when a collimated radio jet is present. As has already been described by Capetti et al. (1995a), the narrow-line region of Mrk 3 shares the morphology of its twin radio jets. In Mrk 348, the northwest side has a linear jetlike morphology in both radio and line emission. On the eastern side of Mrk 78, this picture is less convincing; while it is true that this lobe is substantially more compact than the western lobe, it does not really appear to have a jetlike morphology.

This dichotomy in emission-line morphology suggests that bow shock emission-line structures are produced by the sweeping-up of gas at the advancing working surface of the ejected radio plasma, in the manner described by Taylor et al. (1992). The observed corrugated structure, particularly evident in Mrk 573 and Mrk 78, seems to indicate that instabilities have developed in the compressed gas. Since the advancing radio lobes are in overpressure compared to the surrounding gas, they will expand as they move outward, and this can result in the formation of enshrouding shells of gas as described by Pedlar, Unger, & Dyson (1985). This is a natural explanation for the observed shell-like morphologies seen in the results presented here. The kinematic evidence presented by Pedlar et al. (1989) for Mrk 78, which shows more rapid expansion on the western lobe, is consistent with this picture.

The substantial network of diffuse and filamentary emission seen beyond the bright emission-line bow shocks of Mrk 573 can also be explained in this framework. If the density of the ambient gas drops with radius, it is possible that it will come to a point at which the radio lobe can expand catastrophically, and at the same time its surface brightness will drop dramatically. Any swept-up emission-line gas will be faint, and its kinematics will reflect the rapid expansion of the radio lobe. Such behavior has recently been observed in IRAS 04210+040 (Holloway et al. 1995). High-sensitivity radio maps and long-slit spectroscopy with *HST* are necessary to establish if this is the origin of the outer filaments of Mrk 573. The alternative explanation for the extensive diffuse filaments is, as has often been suggested for Seyfert galaxies (Baum et al. 1993), a consequence of an interaction with a more diffuse thermal wind.

On the other hand, a Seyfert radiojet is enshrouded by a halo of hot gas which expands radially from the jet axis, and the emission lines form a cylindrical cocoon on the outer cooling surface. Therefore, the NLR appears as a linear structure superimposed onto the radio jet.

For Mrk 3, Mrk 573, and Mrk 78, it is possible to explore the physical condition of the emitting gas by analyzing the line emission ratio images.

In Mrk 3, Capetti et al. (1995a) reported that the [O III]/[O II] and the [O III]/Hβ ratios are constant over the jetlike region of the NLR but were significantly lower on the western hotspot. The results presented here confirm these conclusions. A similar situation appears to be occurring in Mrk 78, with high ionization in the eastern lobe associated with the radiojet and much lower ionization in the gas cocoon around the western radio lobe.

In the case of Mrk 573, as discussed in § 3.1.1, the emission-line ratios [O III]/[O II] and [O III]/Hα are essentially constant with the innermost 2".5 ([O III]/[O II] $\sim$ 3 and [O III]/H$\alpha \sim$ 1.5) and [O III]/H$\alpha \sim$ 1.5), and they increase by $\sim$ 30% on the outer filaments at which [O III]/[O II] $\sim$ 4 and [O III]/H$\alpha \sim$ 2. This implies that the ionization parameter increases with radius.

The ground-based observations of Mrk 573 by Tsvetanov & Walsh (1992) indicate that the density decreases from $\sim$800 cm^{-3} at a radius of 1" to $\sim$200 cm^{-3} at 4". If there is no local source of ionization, due to geometrical dilution of the ionizing nuclear radiation field, the ionization parameter should vary as $U_e \propto n_e^{-1} r^{-2}$, and it should therefore decrease by a factor of 4 between 1" and 4".

It appears that an additional source of ionization is required to explain these results. Sutherland et al. (1993) have argued that ionizing emission can be produced in the hot gas which results from the interaction of the radio plasma with the surrounding medium; direct evidence for an extended UV emission in Seyfert galaxies has been reported recently by Capetti et al. (1995b) supporting this interpretation. The detailed ionization structure of the NLR at any radius will depend on the relative performance of the local and nuclear contribution to the radiation field. It is important to realize that the luminosity of the locally produced radiation can be many orders of magnitude lower than that produced in the nucleus and still radically affect the observed ionization structure. This is because the NLR

© American Astronomical Society • Provided by the NASA Astrophysics Data System

1996ApJ...469..554C

clouds subtend a much larger solid angle to the lower ionization source. In principle, the relative importance of the two ionization sources can be determined by studying the variation of the diagnostic line ratios in conjunction with self-consistent photoionization models with the radius, as the nuclear radiation field is geometrically diluted. This requires high-quality long-slit spectroscopy covering a wide range of ionization species, and it is clearly beyond the scope of this paper.

An interesting caveat of this discussion is the quite different ionization seen in the lobes of Mrk 573 compared to those of Mrk 78 and Mrk 3, suggesting that there is indeed a different ionization balance in the sense that the local contribution is lower in the lobes of Mrk 78 and Mrk 3.

Unfortunately, we do not have any information on the ionization structure of Mrk 348 to verify whether it also follows the same trend as the other three galaxies.

5. IMPLICATION ON THE STRUCTURE OF THE CONTINUUM EMISSION

Several species of evidence indicate that a compact torus obscures the active nucleus in Seyfert 2 galaxies (see, Antonucci & Miller 1985; Baldwin 1987; Tadhunter & Tsvetanov 1989). In the case of Mrk 3 and Mrk 78, Capetti et al. (1994, 1995a) showed, by using the photon budget arguments, that the nucleus is indeed obscured. Further support for this scenario is contained in the four continuum images presented in the previous sections, as there is a conspicuous lack of any unresolved source that might be identified with the active nucleus.

In the three closest objects, Mrk 573, Mrk 3, and Mrk 348, a sharp absorption feature, with a thickness between 20 and 50 pc, runs perpendicular to the major axis of the NLR.

In the case of Mrk 573, the continuum emission is bright enough to outline the absorption to $\sim$250 pc from the nucleus, and it is clearly warped. In Mrk 3 and Mrk 348, the surface brightness of the galaxy continuum is insufficient to detect the dust lane outside the bright emission-line region.

In Mrk 78, there is also a central dust lane, but it is substantially thicker, $\sim$180 pc, than those observed in the other galaxies and is inclined with respect to the axis of the NLR. It forms a part of a much more extended network of obscuring material which covers most of the nuclear region.

It appears that in Seyfert type 2, the hidden active nucleus is associated with the presence of a nuclear absorption feature. We suggest that there is a continuity between the torus which is obscuring the nucleus and these more extended nuclear dust lanes. An important step in substantiating this interpretation would be to locate the center of symmetry of the scattered radiation (e.g., by using imaging polarimetry) and to demonstrate that, as in NGC 5728 (Capetti et al. 1996), this center falls indeed in the dust lane.

Recently, inner stellar bars have been found in the infrared in a number of active galaxies (Shaw et al. 1995), and in the case of NGC 5728, the *HST* images show that the NLR is nearly aligned with the inner bar (Wilson et al. 1993). Robinson et al. (1994) and Vila-Vilaro et al. (1995) have presented arguments that inner bars play an important role in the formation of the molecular tori and enhance the formation of collimated radiation fields. We presented evidence in this paper for both large-scale bar structure and nuclear bars in Mrk 573, Mrk 78, and Mrk 3. While there is no doubt that the large-scale bars are indeed stellar in origin, the situation is less clear for the inner bars Capetti et al. (1996) have already argued that in the case of Mrk 3, the inner bar is the manifestation of free-free radiation caused by the interaction of the radio ejecta with the surrounding gas.

From the morphological point of view, the clearest case is Mrk 573, which is rather reminiscent of NGC 5728. In the red continuum, it has two bars nearly perpendicular in projection. The axis of the NLR is close to that of the inner bar but is displaced by $\sim$35°, and this suggests that its inner bar is stellar. Mrk 573 also shows extended UV continuum but, as in Mrk 3, this is cospatial with the brightest region of the NLR. Its fan-shaped morphology suggests that this is either scattered light or a radiation cone.

Both Mrk 78 and Mrk 348 show extended continuum, but again it is cospatial with the emission-line structure, and therefore we cannot distinguish which mechanism is responsible for its origin).

High-resolution infrared imaging is necessary to establish which, if any, of these bars are in fact stellar.

6. SUMMARY

We present the results of *Hubble Space Telescope* observations of four Seyfert 2 galaxies, Mrk 573, Mrk 348, Mrk 3, and Mrk 78, all showing extended radio emission. Images were taken with the Faint Object Camera with filters centered on the oxygen emission lines [O II] λ3727 and [O III] λ5007 and on the visual continuum.

In all four objects there is a close association between the emission-line morphology and the radio emission. These results are strong evidence that the line-emitting gas in the NLR is compressed by shocks created by the passage of the radio-emitting outflow. The increase in the density due to the shocks causes the line emission to be highly enhanced in the region in which this interaction occurs. The morphology of the NLR depends on that of the radio emission. Radio lobes are surrounded by shell-like emission-line structures, probably produced by the sweeping-up of gas by the expanding radio lobe; the emission-line bubbles also show corrugations, which might be due to instabilities in the compressed gas. On the other hand, the line emission lies along the whole length of radio jets. This suggests that the emission lines are created by the expansion of the cylindrical hot cocoon of material around the jet axis.

In the case of Mrk 573, the ionization parameter increases slightly with radius. The density profile across the NLR obtained from ground-based measurements implies that, due to geometrical dilution of the ionizing nuclear radiation field, a decrease by a factor of 4 between 1″ and 4″ in the ionization parameter would be expected. It appears that an additional local source of ionization is required to maintain a higher ionization state at large radius. Local ionizing emission can be produced in the hot gas which results from the interaction of the radio plasma with the surrounding medium.

There is no evidence, in any of these galaxies, for an unresolved bright source which could be identified as the active nucleus, which, we conclude, must be hidden along our line of sight. In all four objects, an absorption feature across the nuclear region has been detected, typically with a scale height of less than 50 pc. It appears that in Seyfert 2 galaxies the hidden active nucleus is associated with the presence of a nuclear absorption feature. This is, therefore, direct evidence for obscuring material which covers the Seyfert nucleus.

© American Astronomical Society • Provided by the NASA Astrophysics Data System

1996ApJ...469..554C

Three of the objects (Mrk 573, Mrk 3, and Mrk 78) show large-scale stellar bars, and Mrk 573 also shows an inner bar oriented nearly perpendicular to the outer bar. Both Mrk 3 and Mrk 78 also show features that might be attributed to nuclear bars; however, in these two cases it is more likely that they are due to continuum emission from gas in the NLR. If the axis of any real inner stellar bar represents a preferred direction for both the radiation field and the radio eject in Seyfert galaxies, this is a vital clue about how these collimated processes are regulated by gas flows fueling the active nucleus.

A. C. acknowledges financial support from the StScI grants GO-4666 and GO-3594.

REFERENCES

Antonucci, R. R. J., & Miller, J. S. 1985, ApJ, 297, 621
Axon, D. J., Dyson, J. E., & Pedlar, A. 1993, in The Nature of Compact Objects in AGN, ed. A. Robinson & R. J. Terlevich (Cambridge: Cambridge Univ. Press), 66
Baldwin, J. A., Wilson, A. S., & Whittle, M. 1987, ApJ, 319, 84
Baum, S. A., O'Dea, C. P., Dellacasa, D., de Bruyn, A. G., & Pedlar, A. 1993, ApJ, 419, 553
Capetti, A., Axon, D. J., Macchetto, F. D., Sparks, W. B., & Boksenberg, A. 1995b, ApJ, 446, 155
———. 1996, ApJ, in press
Capetti, A., Macchetto, F. D., Axon, D. J., Sparks, W. B., & Boksenberg, A. 1995a, ApJ, 448, 600
Capetti, A., Macchetto, F. D., Sparks, W. B., & Boksenberg, A. 1994, ApJ, 421, 87
Clements, E. D. 1981, MNRAS, 197, 829
Evans, I. N., Ford, H. C., Kinney, A. L., Antonucci, R. R. J., Armus, L., & Caganoff, S. 1991, ApJ, 369, L21
Evans, I. N., Tsvetanov, Z., Kriss, G. A., Ford, H. C., Caganoff, S., & Koraktar, A. P. 1993, ApJ, 417, 64
Ferland, G. J., & Osterbrock, D. E. 1986, ApJ, 300, 658
Haniff, C. A., Wilson, A. S., & Ward, M. J. 1988, ApJ, 334, 104
Holloway, A. J., Steffen, W., Pedlar, A., Axon, D. J., Dyson, J. E., Meaburn, J., & Tadhunter, C. N. 1995, MNRAS, in press
Koski, A. T. 1978, ApJ, 223, 56
Kukula, M. J., Ghosh, T., Pedlar, A., Schilizzi, R. T., Miley, G. K., de Bruyn, A. G., & Saikia, D. J. 1993, MNRAS, 264, 893
Macchetto, F., Capetti, A., Sparks, W. B., Axon, D. J., & Boksenberg, A. 1994, ApJ, 435, L15
Neff, S. G., & de Bruyn, A. G. 1983, A&A, 128, 318
Nota, A., Jedrzejewski, R., Greenfield, P., & Hack, W. 1994, Faint Object Camera Instrument Handbook Version 5.0 (Baltimore: Space Telescope Science Institute)
Pedlar, A., Unger, S. W., & Dyson, J. E. 1985, MNRAS, 214, 463
Pedlar, A., Meaburn, J., Axon, D. J., Unger, S. W., Whittle, D. M., Meurs, E. J. A., Guerrine, N., & Ward, M. J. 1989, MNRAS, 238, 863
Robinson, A., Axon, D. J., Perez, E., & Vila-Vilaro, B. 1994, in The Oxford Astrophysics Workshop on Evidence for the Torus, ed. M. J. Ward (Amsterdam: Elsevier) 128
Shaw, M. A., Axon, D. J., Probst, R., & Gatley, I. 1995, MNRAS, 274, 369
Sutherland, R. S., Bicknell, G. V., & Dopita, M. A. 1993, ApJ, 414, 506
Tadhunter, C., & Tsvetanov, Z. 1989, Nature, 341, 422
Taylor, D., Dyson, J. E., & Axon, D. J. 1992, MNRAS, 255, 351
Tsvetanov, Z., & Walsh, J. R. 1992, ApJ, 386, 485
Unger, S. W., Pedlar, A., Neff, S. G., & de Bruyn, A. G. 1986, MNRAS, 209, 15
Vila-Vilaro, B., et al. 1995 A&A, 302, 58
Whittle, M., Pedlar, A., Meurs, E. J. A., Unger, S. W., Axon, D. J., & Ward, M. J. 1988, ApJ, 326, 125
Wilson, A. S., Braatz, J. A., Hecksman, T. M., Krolik, J. H., & Miley, G. K. 1993, ApJ, 419, L61
Wilson, A. S., & Ulvestad, J. S. 1983, ApJ, 275, 8

© American Astronomical Society • Provided by the NASA Astrophysics Data System